Composites: Part A 203 (2026) 109552

Contents lists available at ScienceDirect

Composites Part A

journal homepage: www.elsevier.com/locate/compositesa

Evaluation of the informed isotropic (IISO) viscosity model for compression molding of discontinuous fiber reinforced polymers

Louis Schreyer *, Constantin Krauß, Florian Wittemann, Luise Kärger

Institute of Vehicle Systems Technology, Karlsruhe Institute of Technology (KIT), Germany

ARTICLE INFO

Keywords:
Anisotropic viscosity
Rheology
LFT
SMC
GMT

ABSTRACT

The informed isotropic (IISO) viscosity model has gained popularity as a surrogate for fourth-order tensor viscosity models in simulating injection and compression molding of discontinuous fiber reinforced composites in industrial applications, primarily to overcome numerical challenges that are especially pronounced in long fiber reinforced materials. In addition, the IISO model can be easily integrated into (commercial) isotropic frameworks. The central idea is to equate the energy dissipation rates resulting from a fully anisotropic and an isotropic viscous material model, which allows deriving a scalar surrogate viscosity that depends on the local fiber orientation. However, the model's fundamental capability to predict anisotropic flow behavior in compression molding remains limited. This work comprehensively assesses the IISO viscosity model's capabilities through analytical and numerical investigations of fundamental flow scenarios. We demonstrate that the IISO viscosity model cannot generate elliptical deformation in lubricated squeeze flow of initially cylindrical samples with spatially homogeneous and anisotropic initial fiber orientation states, confirming the model's inherent limitation due to stress–strain-rate coaxiality. When we extend the analysis to non-lubricated squeeze flow, the results emphasize that the IISO viscosity model also fails to produce anisotropic flow regardless of the spatially homogeneous and (aligned) orthotropic initial fiber orientation state. Furthermore, we demonstrate that the compression-molding-style center-gated disk benchmark is inconclusive, as the flow trajectory depends on the magnitude of the imposed perturbation rather than the fiber orientation. The perturbation also introduces a physically implausible circumferential vortex. Finally, we discuss potential sources of apparent anisotropic behavior in numerical flow simulations in the literature and highlight the challenges of parameterizing the IISO viscosity model experimentally.

1. Introduction

1.1. Motivation and state of the art

Compression molding of discontinuous fiber reinforced composites is a widely used manufacturing process for producing complex (semi-)structural components. Compared to injection molding, the fiber length is considerably longer, thereby improving mechanical properties. Common materials include in-line compounded long fiber reinforced thermoplastics (LFT-D), glass mat thermoplastics (GMT), and sheet molding compounds (SMC), selected based on application-specific requirements. While the fiber reinforcement enhances the mechanical properties of the composite [1–3], it also introduces strong fiber orientation dependent behavior. Both, structural and rheological behavior are significantly influenced by the local fiber orientation and its interaction with the surrounding matrix. The anisotropic rheological behavior has been demonstrated in squeeze flow experiments for various materials: bundle-like thermoplastics [4], GMT [5,6], and LFT-D [7], where initially cylindrical samples deform elliptically. In contrast, SMC samples generally retain the circular shape due to the planar isotropic fiber orientation before testing [8,9], though their flow behavior remains fiber-orientation dependent [10].

Accurate prediction of mold filling and resulting fiber orientation requires models that capture the two-way fiber–matrix coupling. Even for short fibers typical in injection molding, this interaction significantly affects the final fiber orientation distribution [11]. To capture this behavior, several anisotropic viscous constitutive models have been developed. These are motivated either by fluid mechanics [12–14] or solid mechanics [15–17] and are applied across a range of discontinuous fiber-reinforced materials [18–20]. However, fully anisotropic models often suffer from numerical issues such as poor system conditioning and convergence problems [21–25].

* Corresponding author.
E-mail address: louis.schreyer@kit.edu (L. Schreyer).

https://doi.org/10.1016/j.compositesa.2025.109552
Received 7 November 2025; Received in revised form 19 December 2025; Accepted 31 December 2025
Available online 8 January 2026

To mitigate these issues, several simplified scalar viscosity models have been proposed in recent literature to reduce the anisotropic viscosity tensor to a scalar surrogate viscosity, which is easier to handle numerically. Costa et al. [26] introduce a threshold-based approach to consider the influence of fiber orientation on the composite's viscosity. However, this approach is not thermodynamically conservative. An alternative is the informed isotropic (IISO) viscosity model proposed by Favaloro et al. [27], which is thermodynamically consistent. In this model, the energy dissipation rate of a fully anisotropic fourth-order tensor model and an isotropic scalar model are equated to obtain a scalar surrogate viscosity. Although the model fails to predict anisotropic behavior in lubricated squeeze flow between two parallel plates, the authors present a simplified verification case, namely a compression-molding-style center-gated disk (CGD), both analytically and via Moldex3D simulations [27]. Simultaneously, Li and Luyé [28] proposed an equivalent model. However, we will refer to the model as IISO viscosity model, as it is commonly known in the literature. Subsequently, the IISO viscosity model has been utilized in prepreg platelet molding [29], compression molding of hybridly laminated thermoplastics [30], GMT [31], SMC [32] and injection molding [33–35].

Motivated by numerical instabilities encountered in an earlier work [23], Tseng and Favaloro [33] propose a full IISO constitutive equation that also introduces shear rate dependence to the parameter describing the anisotropy. The IISO constitutive model is applied to several injection molding examples including a comparison with the isotropic solution and the surrogate viscosity model by Li and Luyé [28]. Building on this, Huang and Lai [34] employed the IISO constitutive equation to examine its influence on fiber orientation and mold filling in injection molding of short fiber reinforced thermoplastics. Both works report the development of a concave flow front pattern in conjunction with the IISO viscosity model, compared to a flat flow front pattern in the isotropic case. However, comparison with the respective fully anisotropic model [33], in which the tensorial information is not reduced to a scalar, are not provided.

In an optimization framework, Rienesl et al. [35] use the IISO constitutive equation in Moldex3D to identify material parameters describing fiber reorientation and anisotropy in short fiber injection molding. However, the objective function only accounts for fiber orientation at discrete locations, resulting in non-unique solutions and parameter sets that depended on the spatial weighting of measurement points.

Favaloro and Sommer [29] apply the IISO viscosity model to prepreg platelet compression molding using Moldex3D, following their earlier smooth particle hydrodynamics (SPH) based work [19] in Abaqus/Explicit, in which a fully anisotropic viscosity model [27] was utilized. The switch to Moldex3D is motivated by challenges with time step restrictions in the SPH solution resulting from the fine particle discretization required to accurately capture shearing near the mold interface under a no-slip boundary condition. In [29], the IISO constitutive equation from Tseng and Favaloro [33] is used, though the anisotropy parameter is not modeled as shear rate dependent. A direct comparison between the informed and the fully anisotropic models is not provided in [29].

Lee et al. [30] employed the IISO viscosity model to simulate discontinuous fiber reinforced layers within a hybridly laminated thermoplastic compression molding process in Abaqus/Explicit. To verify their implementation, the authors simulate lubricated squeezing of an initially cylindrical sample with unidirectional fiber orientation. However, the simulation produces an elliptical deformation, contradicting the analytical prediction in [27].

For the study on GMT compression molding in Dörr et al. [31], we collaboratively implemented the IISO viscosity model within Autodesk Moldflow via the API to perform component-scale simulations. The viscous material parameters were determined from oscillatory rheometry using a fully anisotropic constitutive equation. In contrast, Kapshammer et al. [32] determine the viscous material parameters for SMC using squeeze flow experiments. Furthermore, the IISO viscosity model is utilized in the parameter identification. However, due to the planar isotropic initial fiber orientation of SMC, the sample's cylindrical shape is preserved during these tests, offering limited insight into anisotropic flow behavior. Similar to the concerns raised in Rienesl et al. [35], this parameter identification approach does not include flow-induced effects in the optimization. As a result, the derived anisotropy ratio is substantially higher than reported in, e.g., [36]. For this reason, the parameters describing the anisotropy are often approximated analytically [13,37–39], as done in [17,18,31]. However, the applicability of such expressions must be carefully evaluated, as emphasized in [7]. An overview of published studies using the IISO viscosity model is provided in Table 1.

1.2. Originality

In this work, we comprehensively assess the applicability of the informed isotropic (IISO) viscosity model [27] to compression molding of discontinuous fiber reinforced polymers. To this end, we revisit the limiting case of lubricated squeeze flow between two parallel plates, originally emphasized by Favaloro et al. [27], and extend the analysis to non-lubricated squeeze flow. The latter is particularly important for thermoplastic-based material systems, where the high frictional forces at the mold-composite interface are typically idealized by a no-slip boundary condition. We then re-examine the simplified compression-molding-style benchmark of a center-gated disk (CGD), which is intended to showcase the IISO model's capability to induce anisotropic flow behavior. Drawing from these investigations, we evaluate the model's predictive capabilities and limitations, and discuss its practical relevance in light of existing applications summarized in Table 1.

1.3. Notation

Throughout this manuscript the symbolic notation is employed. Vectors are represented by bold lowercase letters, e.g., $\boldsymbol{a}$, second-order tensors by bold uppercase letters, e.g., $\boldsymbol{A}$, and fourth-order tensors by double-struck letters, e.g., $\mathbb{A}$. Tensor contractions of equal order are expressed as, e.g., $(\boldsymbol{AB})_{ij} = A_{ik}B_{kj}$ for second-order tensors and $(\mathbb{AB})_{ijkl} = A_{ijmn}B_{mnkl}$ for fourth-order tensors. The linear mapping of a fourth-order tensor on a second-order tensor is written as $(\mathbb{A}[\boldsymbol{B}])_{ij} = A_{ijkl}B_{kl}$. Scalar products are denoted by a centered dot, e.g., $\boldsymbol{A} \cdot \boldsymbol{B}$ for second-order tensors, while dyadic products are indicated as, e.g., $\boldsymbol{A} \otimes \boldsymbol{B}$. The second-order identity tensor is denoted by $\boldsymbol{I}$, and the fourth-order projection tensor onto symmetric deviatoric tensors is represented by $\mathbb{I}^{\text{dev}}$. The Cartesian coordinate system is spanned by basis vectors $\boldsymbol{e}_1$, $\boldsymbol{e}_2$, and $\boldsymbol{e}_3$, while the cylindrical coordinate system is spanned by $\boldsymbol{e}_r$, $\boldsymbol{e}_\varphi$, and $\boldsymbol{e}_z$, where $\boldsymbol{e}_3 = \boldsymbol{e}_z$.

2. Theoretical background

In this section, we provide a brief overview of fiber orientation modeling and viscous constitutive modeling relevant to this work.

2.1. Fiber orientation description

A single fiber's orientation is described by a unit vector $\boldsymbol{p} \in S^2$, where S^2 denotes the unit sphere. However, modeling the fiber orientation in industrial composites requires a formal description. This is achieved using the fiber orientation distribution function $\Psi(\boldsymbol{p})$, which relates a fiber orientation $\boldsymbol{p}$ to its occurrence probability. Although the fiber orientation distribution function $\Psi(\boldsymbol{p})$ offers a complete statistical characterization, its arbitrary complexity makes it impractical for most numerical methods. To address this, the fiber orientation distribution function is typically represented by its statistical moments given by

Table 1
Chronological overview of studies using the informed isotropic (IISO) viscosity model.

Reference	Application	Software
Favaloro et al. [27]	Injection molding, compression-molding-style center-gated disk	Moldex3D
Favaloro et al. [40]	Compression molding style center-gated disk	Moldex3D
Li and Luyé [28][a]	Injection molding	Moldflow
Tseng and Favaloro [33]	Injection molding	Moldex3D
Huang and Lai [34]	Injection molding	Moldex3D
Favaloro and Sommer [29]	Prepreg platelet compression molding	Moldex3D
Lee et al. [30]	Hybridly laminated thermoplastics	Abaqus/Explicit
Rienesl et al. [35]	Injection molding	Moldex3D
Dörr et al. [31]	Glass mat thermoplastics (GMT)	Moldflow
Kapshammer et al. [32]	Sheet molding compounds (SMC)	Moldex3D

[a] Simultaneously proposed a model equal to the IISO viscosity model [27].

the kth (even) order fiber orientation tensor $\boldsymbol{A}_{\langle k\rangle}$ following the works of Kanatani [41] and Advani and Tucker [42]. The fiber orientation tensor $\boldsymbol{A}_{\langle k\rangle}$ is defined as

$$\boldsymbol{A}_{\langle k\rangle} = \int_{S^2} \Psi(\boldsymbol{p})\boldsymbol{p}^{\otimes k} dS, \tag{1}$$

where $(\cdot)^{\otimes k}$ denotes the kth times dyadic product. In an engineering context, the second- and fourth-order fiber orientation tensors $\boldsymbol{A}$ and $\mathbb{A}$ are of particular interest. The second-order fiber orientation tensor $\boldsymbol{A}$ is generally utilized to model fiber reorientation in flow simulations. However, the respective evolution equation requires knowledge of the fourth-order fiber orientation tensor $\mathbb{A}$ as well. Closure approximations $\mathbb{A} = C(\boldsymbol{A})$ solve these problems by associating a second-order fiber orientation tensor $\boldsymbol{A}$ with exactly one fourth-order fiber orientation tensor. The orthotropy of the second-order fiber orientation tensor $\boldsymbol{A}$ is generally preserved by closure approximations; therefore, the fourth-order tensor $\mathbb{A}$ is also orthotropic. Notable exceptions are the non-orthotropic closures proposed by [43] for planar fiber orientation states.

2.2. Governing equations and viscous constitutive modeling

In (compression) molding simulation of discontinuous fiber reinforced composites, the transient flow of the material is governed by the conservation of mass and momentum, which can be expressed as

$$\frac{\partial \rho}{\partial t} + \nabla \cdot (\rho \boldsymbol{u}) = 0, \tag{2}$$

$$\frac{\partial \rho \boldsymbol{u}}{\partial t} + \boldsymbol{u}\nabla (\rho \boldsymbol{u}) = \nabla \cdot \boldsymbol{\sigma} + \rho \boldsymbol{g}, \tag{3}$$

where ρ is the density, t is the time, $\boldsymbol{u}$ is the velocity field, $\boldsymbol{\sigma}$ is the Cauchy stress tensor, and $\rho\boldsymbol{g}$ is the gravitational force per unit volume. For non-isothermal simulations, the energy conservation equation is also required. The general form of a viscous constitutive model for a (quasi-)incompressible medium is given by

$$\boldsymbol{\sigma} = -p\boldsymbol{I} + \mathbb{V}'\left[\boldsymbol{D}'\right], \tag{4}$$

where p describes the hydrostatic pressure, $\mathbb{V}' = \mathbb{I}^{\mathrm{dev}}\mathbb{V}\mathbb{I}^{\mathrm{dev}}$ is a symmetric deviatoric fourth-order viscosity tensor, and $\boldsymbol{D}' = \mathbb{I}^{\mathrm{dev}}[\boldsymbol{D}]$ is the deviatoric part of the rate of strain tensor $\boldsymbol{D}$. When the constitutive equation is formulated so that the viscous stresses $\boldsymbol{\tau}$ are purely deviatoric, i.e., $\boldsymbol{\tau} = \mathbb{V}'\left[\boldsymbol{D}'\right]$, the pressure p solely describes the spherical contribution, as emphasized in [44]. The simplest form of a viscous constitutive model is the Newtonian model, where the viscosity tensor $\mathbb{V}$ is a scalar multiple of the symmetric deviatoric projection tensor

$$\mathbb{V}' = 2\eta\mathbb{I}^{\mathrm{dev}}. \tag{5}$$

Including dependence on shear rate $\dot{\gamma}$, temperature T, and curing effects α (for thermoset matrix materials) in the scalar viscosity $\eta(\dot{\gamma}, T, \alpha)$ increases the model's physical interpretation. Following Eqs. (4) and (5), the Cauchy stress $\boldsymbol{\sigma}$ and the rate of deformation tensor $\boldsymbol{D}$ are coaxial. Thus, extension-extension, extension-shear, and shear-shear coupling, as evident in experimental studies [4–7,12], are not considered. Therefore, anisotropic viscous constitutive models, whether derived from fluid [12–14] or solid [15–17] mechanics, are required to capture the material's anisotropic behavior. In these models, the viscosity tensor $\mathbb{V}'(\mathbb{A})$ is expressed as a function of the fourth-order fiber orientation tensor $\mathbb{A}$.

3. Informed isotropic (IISO) viscosity model

The idea of the IISO viscosity model is to introduce anisotropic information into an otherwise isotropic framework by adjusting the magnitude of the scalar surrogate viscosity η_{IISO} depending on the local fiber orientation distribution. The central idea, proposed by Favaloro et al. [27], is to equate the energy dissipation rate $\dot{E}_{\mathrm{D}}$ of a fully anisotropic viscous model with that of an isotropic surrogate:

$$\dot{E}_{\mathrm{D}} = \boldsymbol{\tau} \cdot \boldsymbol{D}' = 2\eta_{\mathrm{IISO}}\boldsymbol{D}' \cdot \boldsymbol{D}' = \mathbb{V}'\left[\boldsymbol{D}'\right] \cdot \boldsymbol{D}', \tag{6}$$

where η_{IISO} is the IISO viscosity. Equating the energy dissipation rates ensures a conservative formulation. Rearranging Eq. (6), the IISO viscosity is obtained as

$$\eta_{\mathrm{IISO}} = \boldsymbol{D}' \cdot \mathbb{V}'\left[\boldsymbol{D}'\right]\left(2\boldsymbol{D}' \cdot \boldsymbol{D}'\right)^{-1} = \boldsymbol{d} \cdot \mathbb{V}'[\boldsymbol{d}], \tag{7}$$

where $\boldsymbol{d} = \boldsymbol{D}'\dot{\gamma}^{-1}$ is the normalized rate of deformation tensor. Substituting Eq. (7) into Eq. (4) yields the general form of an IISO constitutive equation:

$$\boldsymbol{\sigma} = -p\boldsymbol{I} + \boldsymbol{d} \cdot \mathbb{V}'[\boldsymbol{d}]\,\boldsymbol{D}'. \tag{8}$$

A generic form of the fourth-order viscosity tensor definitions in [14,27,44] is given as

$$\mathbb{V}' = \eta\left(\mathbb{I}^{\mathrm{dev}} + \beta\mathbb{A}'\right), \tag{9}$$

where $\mathbb{A}' = \mathbb{I}^{\mathrm{dev}}\mathbb{A}\mathbb{I}^{\mathrm{dev}}$ is the deviatoric part of the fourth-order fiber orientation tensor, and β is a parameter describing the anisotropic contribution. The interpretation of the parameter β may vary depending on the derivation context [14,27]. By inserting Eq. (9) into Eq. (7), the scalar surrogate viscosity becomes

$$\eta_{\mathrm{IISO}} = 2\eta\left(1 + \beta\boldsymbol{d} \cdot \mathbb{A}'[\boldsymbol{d}]\right). \tag{10}$$

The term $\boldsymbol{d} \cdot \mathbb{A}'[\boldsymbol{d}]$, referred to as the stretching kernel [27], describes the alignment between the principal direction of deformation and the fiber orientation. Note that since $\boldsymbol{d}$ is purely deviatoric, i.e., $\mathbb{I}^{\mathrm{sph}}[\boldsymbol{d}] = \boldsymbol{0}$, it follows that $\boldsymbol{d} \cdot \mathbb{A}'[\boldsymbol{d}] = \boldsymbol{d} \cdot \mathbb{A}[\boldsymbol{d}]$. The stretching kernel attains its maximum when the flow direction aligns with the major principal direction of the fiber orientation (if present), leading to a higher surrogate viscosity. Conversely, if the flow is perpendicular to the preferred fiber orientation, the kernel is minimized and the viscosity is reduced.

4. Evaluation of the IISO model for anisotropic flow prediction

Squeeze flow between two parallel plates is a fundamental flow scenario in the compression molding of discontinuous fiber reinforced polymers (cf. Fig. 1). In such experiments, circular samples with an initially aligned in-plane fiber orientation exhibit elliptical deformation, as observed for various material systems [4–7]. Fully anisotropic viscosity models are able to accurately capture this behavior, as demonstrated in several studies [7,12,17,45]. This elliptical deformation is characteristic of orthotropic materials under compressive loading. Since common closure approximations preserve the orthotropy of the second-order fiber orientation tensor, fourth-order viscosity models inherently exhibit orthotropic behavior. Consequently, the squeeze flow cases presented below serve to investigate an orthotropic model's inherent capability to induce anisotropic flow.

Generally, a distinction is made between lubricated and non-lubricated squeeze flow. In lubricated squeeze flow, negligible friction at the mold-composite interface results in plug-flow-like behavior, which is modeled by an ideal slip boundary condition and characterized by purely elongational deformation. In contrast, non-lubricated squeeze flow results from high frictional forces at the interface. These forces are typically idealized by a no-slip boundary condition, yielding a combination of elongation and shear. The resulting through-thickness velocity profiles are characteristic of both compression molding and injection molding.

In the following, we first evaluate the IISO viscosity model's ability to induce anisotropic flow analytically for both lubricated and non-lubricated squeeze flow (Section 4.1). Subsequently, we demonstrate these findings with finite element simulations, which also account for fiber reorientation during flow (Section 4.2).

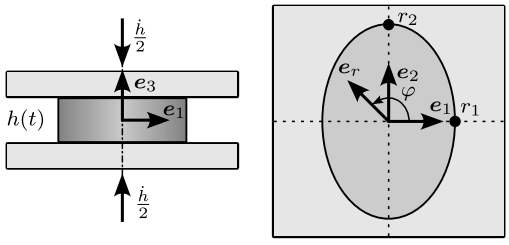

Fig. 1. Schematic of squeeze flow between two parallel plates [7].

4.1. Analytical evaluation

Lubricated squeeze flow. In lubricated squeeze flow, cited as worst-case scenario [27], the IISO viscosity model cannot induce anisotropic flow depending on the fiber orientation, as the model lacks extension-extension coupling. To understand this limitation, we apply a compressive stress $\sigma_{33} = -\hat{\sigma}$ to a continuum with lateral free boundaries. The surface traction at the free boundary

$$\boldsymbol{\sigma n} = \boldsymbol{0},\ \forall\, \boldsymbol{x} \in \partial\Omega_t \tag{11}$$

implies $\sigma_{11} = \sigma_{22} = 0$ at the coordinate axes (cf. Fig. 1), where $\boldsymbol{n}$ is the outward normal vector. Following the definition of the hydrostatic pressure $p = \hat{\sigma}/3$, the deviatoric stresses are $\tau_{33} = \sigma_{33} - p = -2/3\hat{\sigma}$, and $\tau_{11} = \tau_{22} = \hat{\sigma}/3$. In an isotropic framework, the stress tensor and rate of deformation tensor are coaxial, and thus $\tau_{11} = \tau_{22}$ necessitates $D_{11} = D_{22}$. This constraint, however, does not hold for fully anisotropic models.

For further illustration, we analyze the stretching kernel's behavior. The IISO viscosity model alters the magnitude of the scalar viscosity depending on the relative alignment between fiber orientation and rate of deformation. Therefore, the ratio of the stretching kernel between the principal axes $\boldsymbol{d} \cdot \mathbb{A}[\boldsymbol{d}](\varphi = 0)/\boldsymbol{d} \cdot \mathbb{A}[\boldsymbol{d}](\varphi = \pi/2)$ is crucial to the development of anisotropic flow, where φ denotes the circumferential coordinate (cf. Fig. 1). For lubricated squeeze flow of an initially cylindrical sample with spatially homogeneous (orthotropic) fiber orientation, the rate of deformation tensor is given by

$$\boldsymbol{D} = \begin{pmatrix} \dot{\gamma}^0_{11} & 0 & 0 \\ 0 & \dot{\gamma}^0_{22} & 0 \\ 0 & 0 & -\left(\dot{\gamma}^0_{11} + \dot{\gamma}^0_{22}\right) \end{pmatrix}_{\{\boldsymbol{e}_1,\boldsymbol{e}_2,\boldsymbol{e}_3\}}, \tag{12}$$

where $\dot{\gamma}^0_{11}$ and $\dot{\gamma}^0_{22}$ are the rates of deformation at the principal axes (cf. Fig. 1). Since the rate of deformation tensor has no spatial dependence for cylindrical samples, the stretching kernel is spatially uniform even for aligned fiber orientation distributions, provided they are spatially homogeneous.

Non-lubricated squeeze flow. In the following, we extend the above analysis to non-lubricated squeeze flow building upon Ericsson's analytical model [12]. Recently, we proposed an extension to this model that also considers shear thinning [7]. However, for the sake of simplicity, we focus on the original model with the following assumptions, which do not influence the occurrence or non-occurrence of an anisotropic flow:

- Quasi-Newtonian material is assumed incompressible ($\nabla \cdot \boldsymbol{u} = 0$) and exhibits IISO constitutive behavior according to Eq. (10).
- Temperature field is homogeneous ($\nabla T = \boldsymbol{0}$) and isothermal ($\frac{\mathrm{d}T}{\mathrm{d}t} = 0$).
- Inertia effects are negligible ($\rho \frac{\mathrm{D}\boldsymbol{u}}{\mathrm{D}t} \ll \nabla \cdot \boldsymbol{\sigma}$).
- Gravitational forces are neglected ($\rho \boldsymbol{g} = \boldsymbol{0}$).
- Fiber orientation distribution $\boldsymbol{\Psi}$ is orthotropic, i.e., the material also exhibits orthotropic behavior. Furthermore, the material's orthotropy axes coincide with the coordinate axes.
- Initial fiber orientation distribution $\boldsymbol{\Psi}_0$ is spatially homogeneous ($\nabla \boldsymbol{\Psi}_0 = \boldsymbol{0}$).

Since the exact influence of the IISO viscosity model on the velocity field is unknown, we make the following approach for the velocity field:

$$\boldsymbol{u} = \begin{pmatrix} \dot{\gamma}^0_{11}\left(1 - f(x_3)\right) x_1 \\ \dot{\gamma}^0_{22}\left(1 - f(x_3)\right) x_2 \\ -\left(\dot{\gamma}^0_{11} + \dot{\gamma}^0_{22}\right)\left(1 - \frac{1}{\chi} f(x_3)\right) x_3 \end{pmatrix}_{\{\boldsymbol{e}_1,\boldsymbol{e}_2,\boldsymbol{e}_3\}}, \tag{13}$$

where $f(x_3)$ describes the through-thickness profile. Because of the problem's symmetry with respect to the $1,2$-plane, we define the velocity field in the interval $x_3 \in [0, h/2]$, and demand smooth symmetries, i.e., $f'(x_3 = 0) = 0$, where f' corresponds to the total derivative. Inserting Eq. (13) in the mass conservation yields an ordinary differential equation for $f(x_3)$. Imposing the boundary condition $f(h/2) = 1$ at the plate interface yields the following expression for the through-thickness profile:

$$f(x_3) = x_3^{(\chi-1)} \left(\frac{h}{2}\right)^{(1-\chi)}, \tag{14}$$

where $h(t)$ is the transient sample height and $\chi = f(\mathbb{A}, \eta, \beta) \in [3, \infty)$ is a parameter describing the shape of the through-thickness profile. For $\chi \geq 3$, the velocity field is twice differentiable with respect to x_3 in the midplane ($x_3 = 0$), i.e.,

$$\chi \geq 3 \Rightarrow \exists\ \frac{\partial^2}{\partial x_3^2} f(x_3)\bigg|_{x_3=0}. \tag{15}$$

For $\chi = 3$, the through-thickness velocity profile is quadratic, as in the original model [12], and for $\chi \to \infty$, the profile resembles lubricated squeeze flow (cf. Fig. 2). The rate of deformation tensor $\boldsymbol{D}$, calculated from Eqs. (13) and (14), is given in cartesian coordinates $\{\boldsymbol{e}_1, \boldsymbol{e}_2, \boldsymbol{e}_3\}$ as:

$$D_{ij} = \begin{pmatrix} \dot{\gamma}^0_{11}\left(1 - f(x_3)\right) & 0 & -\frac{1}{2}\dot{\gamma}^0_{11} f'(x_3) x_1 \\ & \dot{\gamma}^0_{22}\left(1 - f(x_3)\right) & -\frac{1}{2}\dot{\gamma}^0_{22} f'(x_3) x_2 \\ \text{sym.} & & -\left(\dot{\gamma}^0_{11} + \dot{\gamma}^0_{22}\right)\Xi(x_3) \end{pmatrix} \tag{16}$$

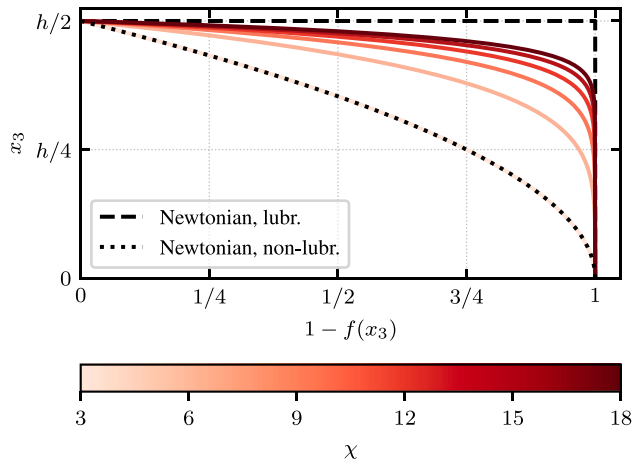

Fig. 2. Normalized through-thickness velocity profiles of u_1 and u_2 for different values of χ.

with $\Xi(x_3) = 1 - 1/\chi\big(f'(x_3)x_3 + f(x_3)\big)$.

Formulating the problem against the midplane ($x_3 = 0$, cf. Fig. 1) takes advantage of the velocity and fiber orientation fields' symmetry, thus, allowing for a manageable model, as noted in [7]. In the midplane, the rate of deformation tensor $\boldsymbol{D}$ is diagonalized and homogeneous, depending only on $\dot{\gamma}^0_{11}$ and $\dot{\gamma}^0_{22}$. Furthermore, the spin tensor is zero, i.e., $\boldsymbol{W}|_{x_3=0} = \boldsymbol{0}$. Consequently, the fiber reorientation $\dot{\boldsymbol{A}} = f(\boldsymbol{D}, \boldsymbol{W})$ in the midplane is also homogeneous and diagonalized as predicted by established evolution equations [42,46,47]. Therefore, the material's orthotropy axes remain aligned with the coordinate system throughout squeezing, which is a fundamental requirement for this analytical approach. Additionally, the fiber reorientation does not contribute to the conservation of momentum in the midplane. Inserting Eq. (16) into the conservation of linear momentum (Lagrange formulation)

$$\nabla p = \nabla \cdot \big(\eta_{\mathrm{IISO}} \boldsymbol{D}\big) = \boldsymbol{D}\nabla\eta_{\mathrm{IISO}} + \eta_{\mathrm{IISO}}\nabla \cdot \boldsymbol{D}, \tag{17}$$

yields the pressure gradient.

Equating the surface traction at the radii $r_1(t)$ and $r_2(t)$ at the coordinate axes

$$\boldsymbol{\sigma n}|_{x_1=r_1, x_2=x_3=0} = \boldsymbol{\sigma n}|_{x_2=r_2, x_1=x_3=0} = \boldsymbol{0}, \tag{18}$$

$$\begin{aligned} -\int_0^{r_1} \frac{\partial p}{\partial x_1}\bigg|_{x_2=x_3=0} \mathrm{d}x_1 + \big(\eta_{\mathrm{IISO}} D_{11}\big)\big|_{\substack{x_1=r_1 \\ x_2=x_3=0}} = \\ -\int_0^{r_2} \frac{\partial p}{\partial x_2}\bigg|_{x_1=x_3=0} \mathrm{d}x_2 + \big(\eta_{\mathrm{IISO}} D_{22}\big)\big|_{\substack{x_2=r_2 \\ x_1=x_3=0}}, \end{aligned} \tag{19}$$

yields a relation between the rates of deformation $\dot{\gamma}^0_{11}$ and $\dot{\gamma}^0_{22}$. For $\chi > 3$, the relation is given by:

$$\frac{\dot{\gamma}^0_{22}}{\dot{\gamma}^0_{11}} = 1, \forall \chi > 3. \tag{20}$$

For $\chi = 3$, it follows analogously:

$$\frac{\dot{\gamma}^0_{22}}{\dot{\gamma}^0_{11}} = \frac{2r_1^2 + h^2}{2r_2^2 + h^2}. \tag{21}$$

However, in both cases, the relation is independent of the fiber orientation. Consequently, the IISO viscosity model also does not predict elliptical deformation for cylindrical samples in non-lubricated squeeze flow for any spatially homogeneous, (aligned) orthotropic fiber orientation state based on this analysis. For initially cylindrical samples, note that the principal axes of the resulting ellipse (which in this case remains circular) always coincide with the material's orthotropy axes.

While the IISO viscosity model does not induce anisotropic flow in the presented cases, it does influence the normal force response. This influence can be attributed to two main effects. First, the IISO viscosity model yields a higher σ_{33} due to the stress–strain-rate coaxiality, provided the fibers are not predominantly oriented out-of-plane, which is unlikely in compression molding. Therefore, the compression force is generally higher in comparison to the fully tensorial model. Second, the IISO viscosity model exhibits a shear-thinning-like effect, resulting in a wider core-region of the velocity profile (see the influence of χ in Fig. 2). Consequently, the slope of the normal force tends to be flatter than that of the fully tensorial model.

4.2. Numerical demonstration

In this section, we numerically demonstrate the findings of Section 4.1 for both lubricated and non-lubricated squeeze flow of an initially cylindrical sample, while also accounting for fiber reorientation during the flow process. The measurements of the sample and the initial fiber orientation are chosen in accordance with the experiments in [7]. Thus, the initial sample height and diameter are 6 mm and 60 mm, respectively. The initial, spatially homogeneous second-order fiber orientation tensor with respect to the sample's orthotropy axes is $\bar{\boldsymbol{A}}_0 = \mathrm{diag}\,(\langle 0.81, 0.19, 0\rangle)$ [7]. To verify that the IISO viscosity model correctly handles general fiber orientation states, the sample's material axes are rotated by $+\pi/4$ with respect to the global coordinate system's 3-direction in the simulation model.

The Folgar-Tucker equation [48] models the evolution of the fiber orientation:

$$\frac{\mathrm{D}\boldsymbol{A}}{\mathrm{D}t} = (\boldsymbol{WA} - \boldsymbol{AW}) + \mu(\boldsymbol{DA} + \boldsymbol{AD} - 2\mathbb{A}[\boldsymbol{D}]) + 2C_{\mathrm{i}}\dot{\gamma}(\boldsymbol{I} - 3\boldsymbol{A}), \tag{22}$$

where μ describes the fiber shape and C_{i} is the empirical interaction coefficient. In this investigation, we chose $\mu = 1$ (large fiber aspect ratio) and $C_{\mathrm{i}} = 0.01$. Compared to Jeffery's equation [49], the additional diffusion in Eq. (22) rotates the fibers towards a more isotropic orientation. Furthermore, the rate of reorientation is also increased for the chosen C_{i} value compared to Jeffery's equation. The fourth-order fiber orientation tensor is approximated by the invariant-based optimal fitting (IBOF) closure $\mathbb{A} \approx \mathbb{A}^{\mathrm{IBOF}}$ [50]. The material's constitutive behavior is modeled with the scalar IISO viscosity model according to Eq. (10). As in Section 4.1, we neglect temperature and shear rate dependence of the viscosity, choosing $\eta = 10^3$ Pa s. To induce strong anisotropic behavior, the parameter describing the anisotropy $\beta = (R_\eta - 1)$ [27] is chosen as $R_\eta = 100$ [7].

The simulations are performed in Abaqus/Explicit using a Lagrangian reference frame. The sample is discretized with linear hexahedron elements (C3D8, cf. Fig. 3). According to the lubricated or non-lubricated squeeze flow case, the boundary conditions are imposed on the nodes at the top and bottom of the sample (cf. Fig. 3). In both cases, compression is prescribed via a velocity boundary condition (smooth step) in the negative 3-direction of the top nodes. Because of the significant element distortion resulting from the no-slip condition in the non-lubricated case, the sample is compressed by ≈14 %, as opposed to 50 % in the lubricated case.

Fig. 4 and Fig. 5 show the numerical contour evolution in lubricated and non-lubricated squeeze flow, respectively. The fully tensorial solutions using Eqs. (4) and (9) are included for reference. When using the IISO viscosity model, the sample maintains a cylindrical shape in both flow scenarios. Therefore, given a spatially homogeneous and orthotropic initial fiber orientation state, fiber reorientation does not lead to anisotropic flow with this approach. In contrast, the fully tensorial model exhibits pronounced elliptical flow in both scenarios. The resulting elliptical deformation causes (severe) localized element distortion, which limits the achievable compression, especially in the non-lubricated case. In all cases, the fibers reorient toward a more isotropic state. However, fiber reorientation is more pronounced in the lubricated case because it undergoes greater overall compression.

Given the larger velocity gradient in the fully tensorial model (elliptical deformation), the fiber orientation at the end of compression is more isotropic compared to the IISO model (circular deformation). Note that, in the fully tensorial model, fiber orientation kinematics tend to reduce the degree of anisotropy and thus the degree of the elliptical deformation.

Additionally, Fig. 6 compares the compression forces predicted by both models. Consistent with the discussion at the end of Section 4.1, the IISO model predicts higher forces for both boundary conditions due to its inherent stress–strain-rate coaxiality. However, the shear-thinning-like effect, which would tend to flatten the force-strain curve, is not apparent in the non-lubricated simulation due to the limited flow path length.

5. Compression molding style center-gated disk

To demonstrate the IISO viscosity model's ability to capture anisotropic behavior given a spatially homogeneous stationary fiber

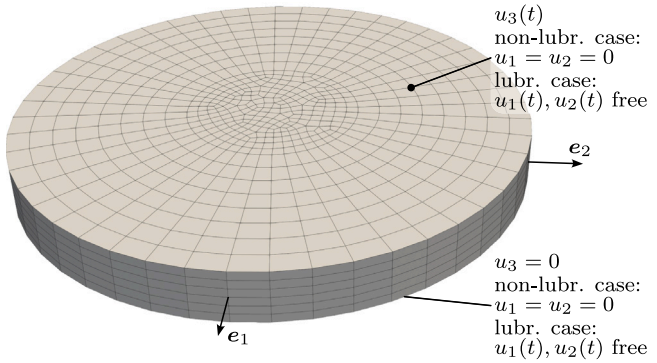

Fig. 3. Finite element model for lubricated and non-lubricated squeeze flow of a cylindrical sample.

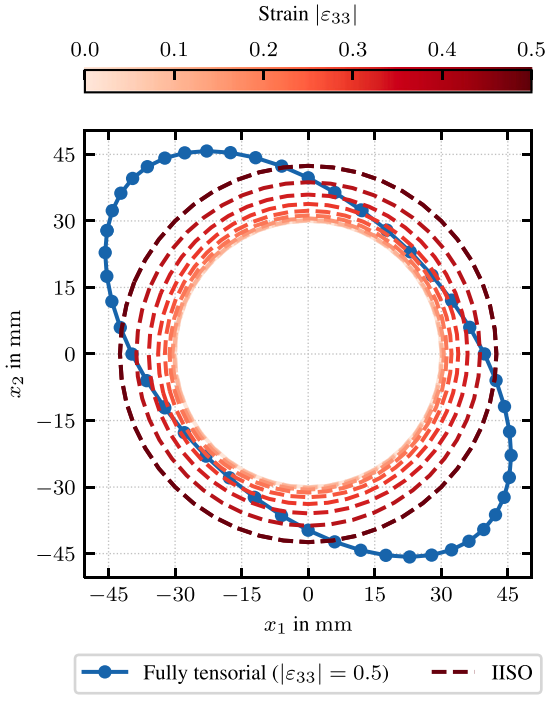

Fig. 4. Numerical flow front evolution in lubricated squeeze flow using the IISO viscosity model, and the resulting contour from the fully tensorial model.

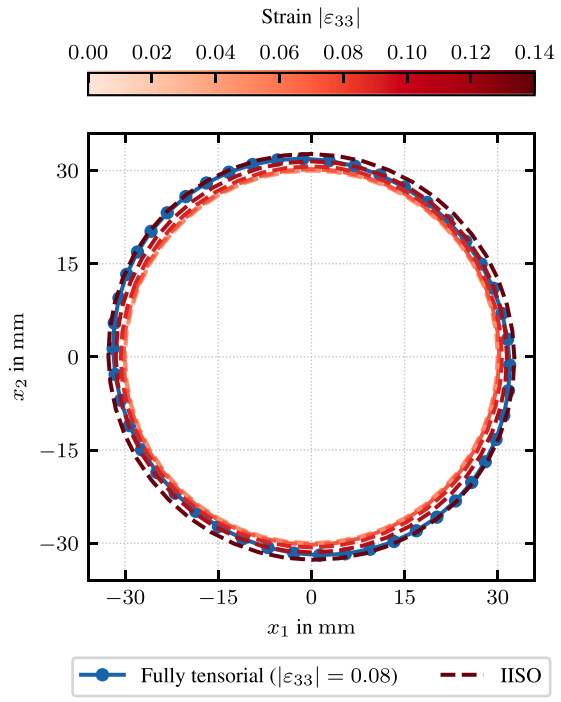

Fig. 5. Numerical flow front evolution in non-lubricated squeeze flow using the IISO viscosity model, and the resulting contour from the fully tensorial model.

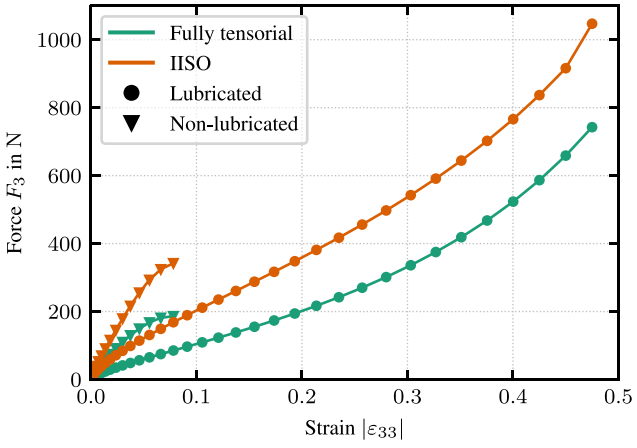

Fig. 6. Numerical compression force predicted by the IISO and fully tensorial model for lubricated and non-lubricated squeeze flow.

orientation state, Favaloro et al. [27] propose a simplification of the lubricated squeeze flow example: a compression-molding-style center-gated disk (CGD) (cf. Fig. 7). In contrast to compression molding, the cavity height h remains constant, and material is injected via a large sprue. To impose strong anisotropic behavior, a homogeneous unidirectional fiber orientation state ($A_{11} = A_{1111} = 1$) is assumed [27].

Three distinct regions are identified in the CGD: the runner where material is placed initially, the cavity that the material fills during molding, and a transition region between the runner and the cavity (light to dark gray in Fig. 7). Within the runner, the material flows downward ($u_3 < 0$), and there is no circumferential or radial velocity ($u_r = u_\varphi = 0$). At a sufficient distance from the injection location, the material only experiences a radial velocity ($u_r > 0$, $u_3 = 0$) as

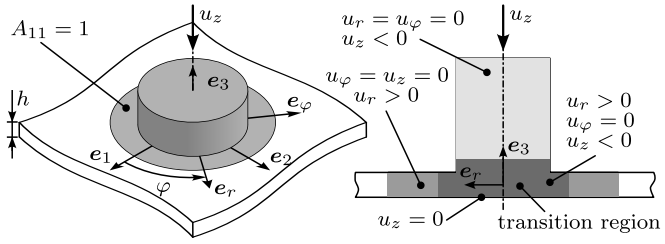

Fig. 7. Schematic of the compression-molding-style center-gated disk (CGD) with stationary unidirectional fiber orientation ($A_{11} = 1$). The distinct regions in the sectional view are (from light to dark gray): the runner, the cavity, and the transition region.

the cavity height is fixed. Thus, a transition region exists, where the material experiences a downward velocity ($u_3 < 0$) and a radial velocity ($u_r > 0$).

To examine the influence of the transition region on the stretching kernel, Favaloro et al. [27] introduce a perturbation to the rate of deformation tensor:

$$\boldsymbol{D}/\dot{\epsilon} = \begin{pmatrix} \xi - 1 & 0 & 0 \\ 0 & 1 & 0 \\ 0 & 0 & -\xi \end{pmatrix}_{\{\boldsymbol{e}_r, \boldsymbol{e}_\varphi, \boldsymbol{e}_z\}}, \tag{23}$$

where ξ quantifies the magnitude of the transition region contribution and $\dot{\epsilon}$ corresponds to a characteristic strain rate that de-dimensionalizes the rate of strain tensor. In cartesian coordinates, the rate of deformation tensor $\boldsymbol{D}$ is given by

$$\boldsymbol{D}/\dot{\epsilon} = \left(\begin{pmatrix} \sin^2\varphi - \cos^2\varphi & 2\sin\varphi\cos\varphi & 0 \\ 2\sin\varphi\cos\varphi & \cos^2\varphi - \sin^2\varphi & 0 \\ 0 & 0 & 0 \end{pmatrix} + \xi \begin{pmatrix} \cos^2\varphi & -\sin\varphi\cos\varphi & 0 \\ -\sin\varphi\cos\varphi & \sin^2\varphi & 0 \\ 0 & 0 & -1 \end{pmatrix} \right)_{\{\boldsymbol{e}_1, \boldsymbol{e}_2, \boldsymbol{e}_3\}}. \tag{24}$$

This representation is obtained via the coordinate transformation $\boldsymbol{D}_{\{\boldsymbol{e}_1,\boldsymbol{e}_2,\boldsymbol{e}_3\}} = \boldsymbol{Q}^T \boldsymbol{D}_{\{\boldsymbol{e}_r,\boldsymbol{e}_\varphi,\boldsymbol{e}_z\}} \boldsymbol{Q}$ with the rotation matrix $\boldsymbol{Q}$.

In the case of unidirectional fiber orientation ($A_{11} = 1$; cf. Fig. 7), the stretching kernel is defined as [27]

$$\boldsymbol{d} \cdot \mathbb{A}[\boldsymbol{d}] = \frac{\left(1 + (\xi - 2)\cos^2\varphi\right)^2}{4\left(\xi^2 - \xi + 1\right)^2}. \tag{25}$$

For $\xi = 0$, the stretching kernel reduces to the planar extension case, yielding isotropic flow. Favaloro et al. [27] argue that a slight perturbation, choosing $\xi = 0.3$, induces a lower viscosity in fiber direction ($\varphi = 0$) compared to the viscosity in transverse direction ($\varphi = \pi/2$), i.e. $\eta_{\text{IISO}}(\varphi = \pi/2) > \eta_{\text{IISO}}(\varphi = 0)$ (cf. Fig. 8(a)). This leads to higher stretching in circumferential direction at $\varphi = \pi/2$ compared to the fiber direction ($\varphi = 0$) [27]. However, the argument could also be made that the smaller surrogate viscosity in fiber direction leads to higher stretching in fiber direction. Furthermore, depending on the magnitude of the perturbation ξ, arbitrary stretching kernel profiles are obtained, as shown in Fig. 8. For $\xi = 2$, the stretching kernel profile is constant, and for $\xi > 2$ the stretching kernel ratio inverts. Thus, the magnitude of the perturbation determines the flow's trajectory. In addition, the definition of the perturbation in Eq. (23) requires a linear dependence of u_φ on φ, i.e., $u_\varphi \propto \varphi$, which behaves similar to a vortex. Moreover, a constant rate of deformation tensor in cylindrical coordinates cannot produce elliptical flow because the necessary periodicity with respect to the φ-coordinate that characterizes elliptical deformation is lacking. Therefore, the perturbation is physically inconsistent, as discussed in more detail in the Appendix.

6. Discussion

Lubricated squeeze flow. Following the analytical investigation in Section 4.1, the IISO viscosity model is unable to induce elliptical deformation of an initially cylindrical sample in lubricated squeeze flow. The compression-molding-style CGD (cf. Section 5) is also not a conclusive counterexample because the perturbation is physically inconsistent, and arbitrary stretching kernel profiles can be generated depending on the size of the perturbation rather than on the initial fiber orientation distribution.

Nevertheless, several works [27,30,40] report simulation results showing elliptical deformation for lubricated squeeze flow of initially cylindrical samples, using different numerical methods. In these works, the IISO viscosity is defined as an explicitly updated field property. While this is natural in the coupled Eulerian Lagrangian (CEL) method with explicit time integration (Abaqus/Explicit) in [30], the IISO viscosity is kept constant throughout each time step in the finite volume based approach in [27,40]. As a result, the IISO viscosity strongly depends on the velocity field at the beginning of the time step, as well as the initial velocity field at the start of the simulation. In addition, in Abaqus/Explicit, the explicit modeling of contact between the composite and plates adds further complexity to the simulation.

Given the theoretical findings (cf. Section 4.1), it is reasonable to conclude that the anisotropic flow observed in such simulations largely results from numerical artifacts, such as highly nonlinear contact modeling, rounding errors, or discretization effects. This conclusion is further supported by the finite element simulations presented in Section 4.2, which model the fundamental flow case of an orthotropic material using a Lagrangian framework. Beyond numerical artifacts, it is possible to impose anisotropic flow by informing the initial velocity field at the beginning of the simulation depending on the fiber orientation state. Unfortunately, the literature lacks direct comparison between the IISO viscosity model and fully tensorial constitutive models. Such comparisons would be feasible for moderate values for the anisotropy parameter β (cf. Eq. (9)), as shown in [17–20] and Section 4.2.

Non-lubricated squeeze flow. In addition to lubricated squeeze flow, the analysis based on Ericsson's model [12] (cf. Section 4.1) further emphasizes that the IISO viscosity model cannot generate anisotropic flow in non-lubricated squeeze flow of cylindrical samples either, regardless of the spatially homogeneous and orthotropic initial fiber orientation state. Thus, an analytical counterexample is available for this flow scenario, which is relevant for thermoplastic composites. Moreover, finite element simulations of this analytical case involving fiber reorientation in a Lagrangian framework corroborate the analytical model's findings, as illustrated in Section 4.2.

IISO viscosity model parameterization. Another key aspect of using the IISO viscosity model is that material parameters determined from fully tensorial models cannot be transferred directly to the IISO framework. The anisotropic flow (if generated due to an initially (non-constant) velocity field or an initially non-homogeneous fiber orientation field) is less pronounced than in the fully tensorial case [27]. In addition, the normal stresses and thus the compression force also differ. Consequently, when restricted to an isotropic framework, the material parameters should be determined specifically using an IISO constitutive model. However, parameterization of any IISO constitutive equation from squeeze flow experiments is not possible using analytical models [7,12], as demonstrated in Section 4.1, because no anisotropic flow develops independent of the homogeneous (and orthotropic) initial fiber orientation state. For the same reason, no simple benchmark case exists that describes the fundamental deformation of an orthotropic material. This absence makes it challenging to (artificially) adjust the anisotropy parameters until sufficient agreement with the fully tensorial model is achieved. To date, no comprehensive discussion regarding this problem is available in the literature. Current approaches for

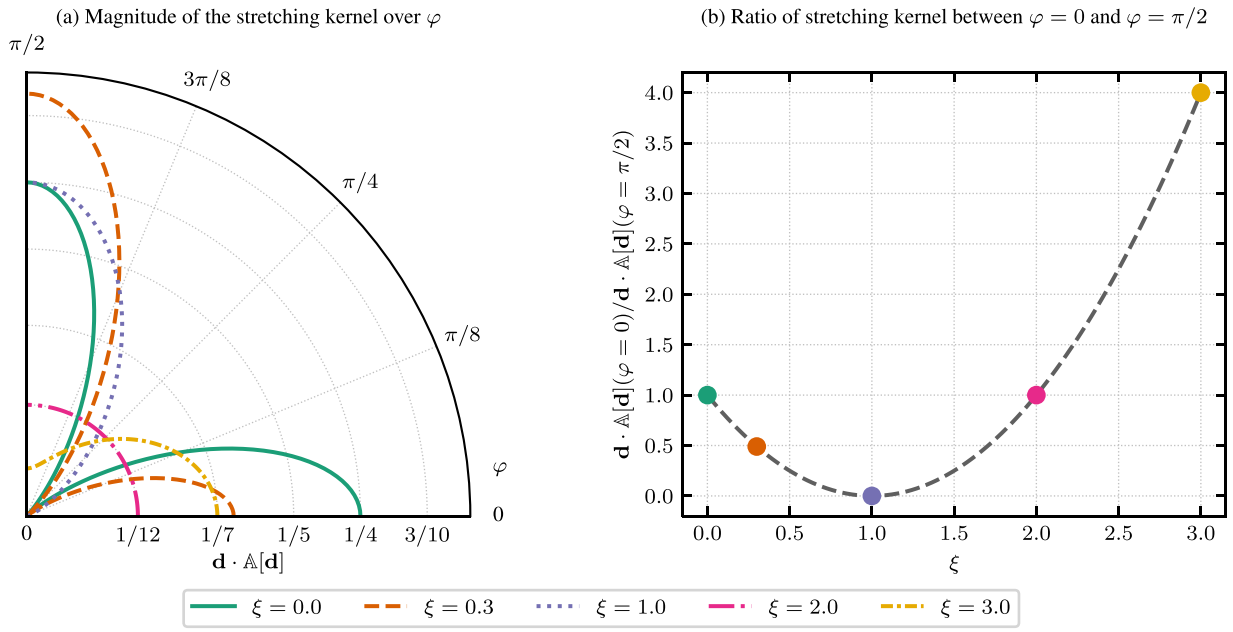

Fig. 8. Behavior of the stretching kernel in compression-molding-style center-gated disk (CGD) with unidirectional fiber orientation ($A_{11} = 1$) depending on the perturbation magnitude ξ (cf. Eq. (25)).

determining the IISO material parameters include: the direct adoption from fully tensorial parameterization [31], component-scale simulations [35], squeeze flow experiments [32], and estimation based on anticipated material behavior [29]. All of these approaches can lead to ambiguous results. While directly adopting from fully tensorial parameterization may significantly underestimate the material anisotropy, parameterization from component-scale simulations is susceptible to numerical artifacts and exhibits strong sensitivity to the choice of experimental sampling locations (leading to optimization convergence to local minima). The challenge is particularly pronounced for material systems without a preferred initial fiber direction (e.g., $A_{11} = A_{22} = 0.5$), such as SMC and GMT, where parameterization from squeeze flow rheometry alone yields ambiguous and physically implausible results, as highlighted by the findings in [32]. This limitation applies equally to both IISO and fully tensorial models because the material deformation remains isotropic in the absence of a preferential (initial) fiber orientation. Consequently, no information about the anisotropic deformation behavior is available, requiring anisotropy parameters to be determined solely from force measurements, which leads to non-unique solutions.

Kinematically informed scalar surrogate model. An alternative approach to develop a scalar surrogate viscosity model is to artificially modify the rate of strain tensor based on the fiber orientation $\boldsymbol{D}^* = f(\mathbb{A})$, i.e., the model is kinematically informed. To ensure physical consistency, the dissipative power (cf. Eq. (6)) must also be preserved. However, such an approach has the disadvantage that it cannot be easily integrated into (commercial) isotropic frameworks since the rate of strain tensor cannot generally be manipulated by the user.

Viscosity model verification cases. Finally, in addition to analytical considerations, we propose two numerical verification cases for scalar surrogate and fully tensorial viscosity models. The first case is lubricated squeeze flow of a cylindrical sample, analyzed within a purely Lagrangian frame of reference, as demonstrated in Section 4.2. With this approach, boundary conditions are directly imposed at the nodes, minimizing numerical errors. The second case expands on the CGD benchmark with initially aligned fiber orientation in [27] by prescribing an isotropic initial velocity field. In this scenario, an anisotropic constitutive model should alter the flow pattern depending on the fiber orientation. Moreover, maintaining a constant gap height, i.e. implementing an injection-induced rather than compression-induced flow, further reduces the influence of numerical artifacts, such as mesh motion and fluid–structure interaction in Eulerian frameworks.

7. Conclusion

First, we investigated and verified the IISO viscosity model's inability to generate elliptical deformation in lubricated squeeze flow (characterized by negligible frictional contact forces) of initially cylindrical samples with an aligned fiber orientation. In addition to basic considerations of a continuum, the model's limitations were illustrated on the basis of the strain rate tensor for planar extension. Furthermore, we extended the discussion to non-lubricated squeeze flow (characterized by substantial frictional contact forces and no-slip) of initially cylindrical samples. We analytically demonstrated that the IISO viscosity model cannot produce anisotropic flow in this essential flow scenario either, regardless of the initial spatially homogeneous fiber orientation state. Finite element simulations using a purely Lagrangian reference frame were conducted for both cases, corroborating the analytical results.

Second, we demonstrated that the counterexample of the compression-molding-style center-gated disk (CGD) is inconclusive, as the flow trajectory depends on the magnitude of the imposed perturbation instead of the (initial) fiber orientation. In addition, the perturbation induces a vortex in the circumferential direction, which is physically implausible.

We then discussed possible reasons for the anisotropic flow in lubricated squeeze flow presented in the literature and emphasized that material parameters determined from fully tensorial models cannot be directly transferred to the IISO framework. Accordingly, no uniform approach for transferring material parameters to an IISO framework is available in the literature.

In conclusion, fully anisotropic (fourth-order tensor) viscosity models should be preferred over the IISO viscosity model for accurate representation of flow-fiber coupling. However, when restricted to an isotropic (commercial) framework, the IISO viscosity model is currently the preferred choice over a simple isotropic material description that neglects the fiber contribution entirely. Nevertheless, when using it, its

limitations must be taken into account: inability to capture anisotropic flow (in fundamental deformation scenarios), deviations in predicted compression forces, and potentially spurious anisotropic flow behavior arising from numerical artifacts.

CRediT authorship contribution statement

Louis Schreyer: Writing – review & editing, Writing – original draft, Visualization, Validation, Software, Methodology, Investigation, Formal analysis, Data curation, Conceptualization. **Constantin Krauß:** Writing – review & editing, Methodology, Conceptualization. **Florian Wittemann:** Writing – review & editing. **Luise Kärger:** Writing – review & editing, Supervision, Project administration, Funding acquisition.

Declaration of competing interest

The authors declare that they have no known competing financial interests or personal relationships that could have appeared to influence the work reported in this paper.

Acknowledgments

The research documented in this manuscript has been funded initially by the German Research Foundation (DFG) as part of the International Research Training Group “Integrated engineering of continuous-discontinuous long fiber reinforced polymer structures” (IRTG 2078), and subsequently by the German Federal Ministry for Economic Affairs and Climate Action (BMWK) as part of the EcoDynamicSMC research project. The work is also part of the Heisenberg project “Digitalization of fiber-reinforced polymer processes for resource-efficient manufacturing of lightweight components” (455807141), funded by the DFG. The support by the DFG, Germany and BMWK is gratefully acknowledged.

Appendix. Analysis of the perturbation definition

In this section, we investigate the definition of the perturbation in Eqs. (23) and (24) of the compression-molding-style CGD (cf. Fig. 7) in more detail. In addition to the incompressibility condition ($\nabla \cdot \boldsymbol{u} = 0$), the individual components of the rate of deformation tensor must follow from the definition of the velocity field. To analyze the latter, we start by computing the radial velocity u_r by integrating D_{rr} (cf. Eq. (23)):

$$u_r = \int D_{rr}\mathrm{d}r = \int (\xi - 1)\mathrm{d}r = (\xi - 1)\, r + g_1(\varphi), \tag{26}$$

where $g_1(\varphi)$ is an integration constant, which can be an arbitrary function of φ. A contribution of the out-of-plane coordinate x_3 to the radial velocity is neglected, as it is not relevant for the following analysis. Assuming that flow only occurs in the region $r > r_0$ and applying the boundary condition $u_r(r = r_0) = 0$ at the onset of the transition region, we obtain

$$u_r = (\xi - 1)\big(r - r_0\big), \forall r > r_0. \tag{27}$$

The use of r_0 as a boundary condition provides a more general formulation than simply using $r = 0$, although $r_0 = 0$ in Fig. 7. To compute the circumferential velocity u_φ, we substitute Eq. (27) into the definition of $D_{\varphi\varphi}$, which follows from the velocity gradient in cylindrical coordinates and the perturbed rate of deformation tensor (cf. Eq. (23)):

$$D_{\varphi\varphi} = \frac{1}{r}\frac{\partial u_\varphi}{\partial \varphi} + \frac{u_r}{r} = 1. \tag{28}$$

This substitution yields the following differential equation:

$$\frac{1}{r}\frac{\partial u_\varphi}{\partial \varphi} + \frac{(\xi - 1)\big(r - r_0\big)}{r} = 1, \tag{29}$$

$$\Rightarrow \frac{\partial u_\varphi}{\partial \varphi} = r - (\xi - 1)\big(r - r_0\big). \tag{30}$$

Integrating Eq. (30) yields the circumferential velocity:

$$u_\varphi = \int \big(r - (\xi - 1)\big(r - r_0\big)\big)\mathrm{d}\varphi = \big(r - (\xi - 1)\big(r - r_0\big)\big)\varphi + g_2(r), \tag{31}$$

where $g_2(r)$ is an integration constant, which can be an arbitrary function of r. The definition of the velocity u_φ contains a linear term in φ that corresponds to a vortex. However, this term cannot be compensated for by $g_2(r)$, making the definition of $\boldsymbol{D}$ unphysical. Furthermore, there is no suitable boundary condition for u_φ that satisfies the differential equations of the remaining components of the strain rate tensor.

In the case of an elliptical deformation (the fundamental geometric shape of an orthotropic material), shearing occurs everywhere except on the coordinate axes (cf. Fig. A.1). Therefore, for physical consistency, the perturbation should also induce deformation in the circumferential components.

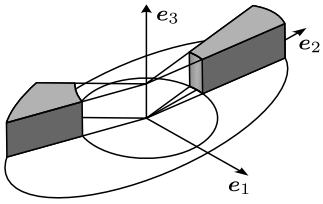

Fig. A.1. Volume elements between and on coordinate axes in elliptical flow of an orthotropic material; volume element between the coordinate axes indicates shear deformation.

Data availability

Data will be made available on request.

References

[1] Bondy M, Pinter P, Altenhof W. Experimental characterization and modelling of the elastic properties of direct compounded compression molded carbon fibre/polyamide 6 long fibre thermoplastic. Mater Des 2017;122:184–96. http://dx.doi.org/10.1016/j.matdes.2017.03.010.

[2] Scheuring BM, Christ N, Blarr J, Liebig WV, Hohe J, Montesano J, Weidenmann KA. Experimental and homogenized orientation-dependent properties of hybrid long fiber-reinforced thermoplastics. Int J Mech Sci 2024;280:109470. http://dx.doi.org/10.1016/j.ijmecsci.2024.109470.

[3] Trauth A, Pinter P, Weidenmann K. Investigation of quasi-static and dynamic material properties of a structural sheet molding compound combined with acoustic emission damage analysis. J Compos Sci 2017;1(2):18. http://dx.doi.org/10.3390/jcs1020018.

[4] Dumont P, Vassal J-P, Orgéas L, Michaud V, Favier D, Månson J-AE. Processing, characterisation and rheology of transparent concentrated fibre-bundle suspensions. Rheol Acta 2007;46(5):639–51. http://dx.doi.org/10.1007/s00397-006-0153-8.

[5] Dweib MA, Ó Brádaigh CM. Anisotropic modeling of isothermal squeezing flow of Glass-Mat reinforced thermoplastics (GMT). Polym Compos 1998;19(5):588–99. http://dx.doi.org/10.1002/pc.10132.

[6] Dweib MA, Ó Brádaigh CM. Compression molding of glass reinforced thermoplastics: Modeling and experiments. Polym Compos 2000;21(5):832–45. http://dx.doi.org/10.1002/pc.10238.

[7] Schreyer L, Krauß C, Scheuring BM, Hrymak A, Kärger L. Characterization and modeling of the anisotropic flow behavior of long carbon fiber reinforced thermoplastic compression molding. Composites A 2025;109053. http://dx.doi.org/10.1016/j.compositesa.2025.109053.

[8] Dumont P, Orgéas L, Le Corre S, Favier D. Anisotropic viscous behavior of sheet molding compounds (SMC) during compression molding. Int J Plast 2003;19(5):625–46. http://dx.doi.org/10.1016/S0749-6419(01)00077-8.

[9] Ferré-Sentis D, Dumont P, Orgéas L, Martoïa F, Sager M. Rheological response of compressible SMCs under various deformation kinematics: Experimental aspects and simple modelling approach. Composites A 2022;154:106774. http://dx.doi.org/10.1016/j.compositesa.2021.106774.

[10] Meyer N, Gajek S, Görthofer J, Hrymak A, Kärger L, Henning F, Schneider M, Böhlke T. A probabilistic virtual process chain to quantify process-induced uncertainties in Sheet Molding Compounds. Composites B 2023;249:110380. http://dx.doi.org/10.1016/j.compositesb.2022.110380.

[11] Karl T, Zartmann J, Dalpke S, Gatti D, Frohnapfel B, Böhlke T. Influence of flow–fiber coupling during mold-filling on the stress field in short-fiber reinforced composites. Comput Mech 2023;71(5):991–1013. http://dx.doi.org/10.1007/s00466-023-02277-z.

[12] Ericsson KA, Toll S, Månson J-AE. The two-way interaction between anisotropic flow and fiber orientation in squeeze flow. J Rheol 1997;41(3):491–511. http://dx.doi.org/10.1122/1.550833.

[13] Dinh SM, Armstrong RC. A rheological equation of state for semiconcentrated fiber suspensions. J Rheol 1984;28(3):207–27. http://dx.doi.org/10.1122/1.549748.

[14] Tucker CL. Flow regimes for fiber suspensions in narrow gaps. J Non-Newton Fluid Mech 1991;39(3):239–68. http://dx.doi.org/10.1016/0377-0257(91)80017-E.

[15] Gibson A. Die entry flow of reinforced polymers. Composites 1989;20(1):57–64. http://dx.doi.org/10.1016/0010-4361(89)90683-6.

[16] Beaussart A, Hearle J, Pipes R. Constitutive relationships for anisotropic viscous materials. Compos Sci Technol 1993;49(4):335–9. http://dx.doi.org/10.1016/0266-3538(93)90064-N.

[17] Sommer DE, Favaloro AJ, Pipes RB. Coupling anisotropic viscosity and fiber orientation in applications to squeeze flow. J Rheol 2018;62(3):669–79. http://dx.doi.org/10.1122/1.5013098.

[18] Wittemann F, Maertens R, Kärger L, Henning F. Injection molding simulation of short fiber reinforced thermosets with anisotropic and non-Newtonian flow behavior. Composites A 2019;124:105476. http://dx.doi.org/10.1016/j.compositesa.2019.105476.

[19] Favaloro AJ, Sommer DE, Denos BR, Pipes RB. Simulation of prepreg platelet compression molding: Method and orientation validation. J Rheol 2018;62(6):1443–55. http://dx.doi.org/10.1122/1.5044533.

[20] Görthofer J, Meyer N, Pallicity TD, Schöttl L, Trauth A, Schemmann M, Hohberg M, Pinter P, Elsner P, Henning F, Hrymak AN, Seelig T, Weidenmann K, Kärger L, Böhlke T. Virtual process chain of sheet molding compound: Development, validation and perspectives. Composites B 2019;169:133–47. http://dx.doi.org/10.1016/j.compositesb.2019.04.001.

[21] Tang L, Altan M. Entry flow of fiber suspensions in a straight channel. J Non-Newton Fluid Mech 1995;56(2):183–216. http://dx.doi.org/10.1016/0377-0257(94)01280-U.

[22] Verweyst BE, Tucker III CL. Fiber suspensions in complex geometries: Flow/orientation coupling. Can J Chem Eng 2002;80(6):1093–106. http://dx.doi.org/10.1002/cjce.5450800611.

[23] Tseng H-C, Su T-H. Coupled flow and fiber orientation analysis for 3D injection molding simulations of fiber composites. AIP Conf Proc 2019;2065(1):030021. http://dx.doi.org/10.1063/1.5088279.

[24] Lipscomb G, Denn M, Hur D, Boger D. The flow of fiber suspensions in complex geometries. J Non-Newton Fluid Mech 1988;26(3):297–325. http://dx.doi.org/10.1016/0377-0257(88)80023-5.

[25] Kobler E, Birtha J, Marschik C, Straka K, Steinbichler G, Schlecht S. Modeling the anisotropic squeeze flow during hot press consolidation of thermoplastic unidirectional fiber-reinforced tapes. J Thermoplast Compos Mater 2023;08927057231214458. http://dx.doi.org/10.1177/08927057231214458.

[26] Costa FS, Cook PS, Pickett D. A framework for viscosity model research in injection molding simulation, including pressure and fiber orientation dependence. In: SPE ANTEC Conference, Technical Papers. Orlando, USA; 2015.

[27] Favaloro AJ, Tseng HC, Pipes RB. A new anisotropic viscous constitutive model for composites molding simulation. Composites A 2018;115(July):112–22. http://dx.doi.org/10.1016/j.compositesa.2018.09.022.

[28] Li T, Luyé J-F. Flow-fiber coupled viscosity in injection molding simulations of short fiber reinforced thermoplastics. Int Polym Process 2019;34(2):158–71. http://dx.doi.org/10.3139/217.3706.

[29] Favaloro AJ, Sommer DE. On the use of orientation tensors to represent prepreg platelet orientation state and variability. J Rheol 2020;64(3):517–27. http://dx.doi.org/10.1122/1.5135010.

[30] Lee S, Shin D, Kim G, Ji W. Numerical model for compression molding process of hybridly laminated thermoplastic composites based on anisotropic rheology. Compos Part C: Open Access 2022;7:100215. http://dx.doi.org/10.1016/j.jcomc.2021.100215.

[31] Dörr D, Singh-Heer N, Gergely RC, Schreyer L, Henning F, Straatman AG, Hrymak A. Rheological characterization and macroscopic modeling and simulation of the molding process of a PA6 Glass Mat Thermoplastic (GMT). Composites A 2024;176:107780. http://dx.doi.org/10.1016/j.compositesa.2023.107780.

[32] Kapshammer A, Huemer-Kals S, Zulueta K, Fischer P, Major Z. An advanced compression molding simulation and validation of a thick-walled carbon fiber sheet molding compound brake caliper. J Manuf Mater Process 2025;9(4):137. http://dx.doi.org/10.3390/jmmp9040137.

[33] Tseng H-C, Favaloro AJ. The use of informed isotropic constitutive equation to simulate anisotropic rheological behaviors in fiber suspensions. J Rheol 2019;63(2):263–74. http://dx.doi.org/10.1122/1.5064727.

[34] Huang C-T, Lai C-H. Investigation on the coupling effects between flow and fibers on fiber-reinforced plastic (FRP) injection parts. Polymers 2020;12(10):2274. http://dx.doi.org/10.3390/polym12102274.

[35] Rienesl K, Stelzer PS, Major Z, Hsu C-C, Chang L-Y, Zulueta K. Determination of fiber orientation model parameters for injection molding simulations via automated metamodel optimization. Front Mater 2023;10:1152471. http://dx.doi.org/10.3389/fmats.2023.1152471.

[36] Le Corre S, Orgéas L, Favier D, Tourabi A, Maazouz A, Venet C. Shear and compression behaviour of sheet moulding compounds. Compos Sci Technol 2002;62(4):571–7. http://dx.doi.org/10.1016/S0266-3538(01)00151-8.

[37] Batchelor GK. Slender-body theory for particles of arbitrary cross-section in Stokes flow. J Fluid Mech 1970;44(3):419–40. http://dx.doi.org/10.1017/S002211207000191X.

[38] Shaqfeh ESG, Fredrickson GH. The hydrodynamic stress in a suspension of rods. Phys Fluids A 1990;2(1):7–24. http://dx.doi.org/10.1063/1.857683.

[39] Pipes RB, Coffin DW, Simacek P, Shuler SF, Okine RK. Rheological behavior of collimated fiber thermoplastic composite materials. In: Flow and Rheology in Polymer Composites Manufacturing. Elsevier Science B.V.; 1992, p. 85–125.

[40] Favaloro AJ, Pipes RB, Tseng H-C. A new anisotropic flow simulation for compression molding of glass-mat thermoplastics. AIP conference proceedings 2019;2065:030038. http://dx.doi.org/10.1063/1.5088296.

[41] Kanatani K-I. Distribution of directional data and fabric tensors. Internat J Engrg Sci 1984;22(2):149–64. http://dx.doi.org/10.1016/0020-7225(84)90090-9.

[42] Advani SG, Tucker CL. The use of tensors to describe and predict fiber orientation in short fiber composites. J Rheol 1987;31(8):751–84. http://dx.doi.org/10.1122/1.549945.

[43] Tucker CL. Planar fiber orientation: Jeffery, non-orthotropic closures, and reconstructing distribution functions. J Non-Newton Fluid Mech 2022;310:104939. http://dx.doi.org/10.1016/j.jnnfm.2022.104939.

[44] Bertóti R. Modeling the flow-induced anisotropic effective viscosity of fiber suspensions by mean-field and full-field homogenization (Dissertation), Karlsruhe Institute of Technology (KIT); 2021, http://dx.doi.org/10.5445/IR/1000131222.

[45] Meyer N. Mesoscale simulation of the mold filling process of Sheet Molding Compound (Dissertation), Karlsruhe: Karlsruhe Institute of Technology (KIT); 2022, http://dx.doi.org/10.5445/KSP/1000143703.

[46] Wang J, O'Gara JF, Tucker CL. An objective model for slow orientation kinetics in concentrated fiber suspensions: Theory and rheological evidence. J Rheol 2008;52(5):1179–200. http://dx.doi.org/10.1122/1.2946437.

[47] Phelps JH, Tucker CL. An anisotropic rotary diffusion model for fiber orientation in short- and long-fiber thermoplastics. J Non-Newton Fluid Mech 2009;156(3):165–76. http://dx.doi.org/10.1016/j.jnnfm.2008.08.002.

[48] Folgar F, Tucker CL. Orientation behavior of fibers in concentrated suspensions. J Reinf Plast Compos 1984;3(2):98–119. http://dx.doi.org/10.1177/073168448400300201.

[49] Jeffery GB. The motion of ellipsoidal particles immersed in a viscous fluid. Proc R Soc Lond Ser A Contain Pap Math Phys Character 1922;102(715):161–79. http://dx.doi.org/10.1098/rspa.1922.0078.

[50] Chung DH, Kwon TH. Invariant-based optimal fitting closure approximation for the numerical prediction of flow-induced fiber orientation. J Rheol 2002;46(1):169–94. http://dx.doi.org/10.1122/1.1423312.